Construction and Building Materials 37 (2012) 15–20

Contents lists available at SciVerse ScienceDirect

Construction and Building Materials

journal homepage: www.elsevier.com/locate/conbuildmat

Strain hardening fiber reinforced alkali-activated mortar – A feasibility study

Bang Yeon Lee [a], Chang-Geun Cho [b,*], Hyun-Jin Lim [b], Jin-Kyu Song [a], Keun-Hyeok Yang [c], Victor C. Li [d]

[a] School of Architecture, Chonnam National University, 300 Yongbong-dong, Buk-gu, Gwangju 500-757, Republic of Korea
[b] School of Architecture, Chosun University, Gwangju, Republic of Korea
[c] Department of Architectural Engineering, Kyonggi University, San 94-6, Iui-dong, Yeongtong-gu, Suwon-si, Gyeonggi-do 443-760, Republic of Korea
[d] Department of Civil and Environmental Engineering, University of Michigan, Ann Arbor, 48109-2125 MI, United States

HIGHLIGHTS

- We present strain-hardening fiber cementless composite mortars.
- The mixtures were determined by alkali-activators and water to binder ratio.
- The cementless fiber composites has high ductility and self-controlled crack width.
- The tensile strain capacities of the mortar ranged from 1.53% to 4.48%.

ARTICLE INFO

Article history:
Received 22 February 2012
Received in revised form 1 June 2012
Accepted 4 June 2012

Keywords:
Alkali-activated mortar
Granulated blast-furnace slag
Sodium sulfate
Calcium hydroxide
Strain-hardening
PVA fiber

ABSTRACT

The development of cementless slag-based alkali-activated mortar has previously been demonstrated. While greener than Portland cement based compositions, slag-based alkali-activated mortar tends to be highly brittle. In the present work, the feasibility of developing a new strain-hardening fiber reinforced composite using slag-based alkali-activated mortar reinforced by polyvinyl alcohol fiber is presented. In the development, three mixtures having a viscosity range that promotes uniform fiber dispersion were determined according to the types of alkali-activator and water to binder ratio. A series of experiments, including density, compression, uniaxial tension and panel bending tests were carried out to characterize the mechanical properties of the composite. Test results establish the feasibility of attaining tensile strain up to 4.7% in fiber reinforced alkali-activated slag composite, compared with 0.020% for the mortar matrix alone.

1. Introduction

Greenhouse gas (GHG) emission is one of the most serious issues worldwide because it is considered the main cause of global warming. Carbon dioxide (CO_2) occupies 82% of the total GHG [1] and the CO_2 produced from the cement industry is up to 7% of global manmade CO_2, although the industry emits almost no other GHGs [2]. Therefore, the production of ordinary Portland cement (OPC) is considered one of the significant contributors to global warming. Various approaches to reducing CO_2 due to cement production has been investigated and some adopted, such as reduction of CO_2 emissions in cement production, reduction of energy consumption in clinker production, and reduction of clinker contents in cement [1]. Since the 1960s, many studies have been carried out to develop cementless slag- or fly ash-based alkali-activated mortar and concrete and to investigate such materials' mechanical and chemical properties [3–8]; it is known that alkali-activated concrete has advantages over OPC concrete, such as high strength development at early and long-term ages, high resistance to chemical attack and freeze–thaw, and lower carbonation rates [3,5]. In addition to enhanced mechanical and durability performances, cementless alkali-activated concrete should also contribute to lowering CO_2 and energy footprints of concrete infrastructure.

The literature on the fracture properties of alkali-activated concrete is fairly limited. Ji [9] measured the fracture energy of two alkali-activated slag concretes. The fracture energies for the two concrete were found to be 167.4 J/m^2 and 186.8 J/m^2, about the same order of magnitude of the fracture energy of OPC concrete [10]. Recent studies reported that alkali-activated mortar or concrete shows similar fracture behavior to OPC mortar or concrete [11–13]. From the previous studies, it is concluded that alkali-activated mortar or concrete are also brittle and susceptible to cracking under tension like OPC mortar or concrete. Cracking increases permeability and allows water, air and aggressive agents such as chloride to reach steel reinforcing steel under the concrete cover,

* Corresponding author. Tel.: +82 622307023; fax: +82 622307155.
E-mail address: chocg@chosun.ac.kr (C.-G. Cho).

0950-0618/$ - see front matter © 2012 Elsevier Ltd. All rights reserved.
http://dx.doi.org/10.1016/j.conbuildmat.2012.06.007

leading to lower durability in reinforced concrete structures. One approach to addressing this problem is the incorporation of fibers, which enables control of cracking and increases the fracture toughness of the brittle matrix through fiber bridging. Silva and Thaumaturgo [12] investigated the effect of fiber volume on the fracture toughness of alkali-activated mortar composite incorporating woolastonite microfibers. Surprisingly the fracture toughness of composite incorporating fibers up to 5 vol.% was same order of magnitude of mortar. Same result was obtained from the study using basalt fibers [13]. This is probably due to the choice of brittle fibers that fractures upon bending forced by crack opening. Thus alkali-activated concrete with high fracture toughness appears not to have been attained as yet. Furthermore, there is a knowledge gap concerning the development of high ductile alkali-activated mortar based composites in the scientific literature. The objective of this study is to experimentally establish the feasibility of developing a new strain-hardening fiber reinforced cementless composite using alkali-activated ground granulated blast furnace slag (GGBS) based mortar and polyvinyl alcohol (PVA) fibers. Such a composite should lead to improved infrastructure durability and resilience as well as material greenness.

2. Experimental investigation

2.1. Materials and mixture composition

The materials and mix proportions investigated in this study are listed in Table 1. The GGBS and the alkali-activator, composed of calcium hydroxide, sodium sulfate and sodium silicate, which come in powder form, were used as binding materials. Calcium hydroxide and sodium sulfate were used as alkali-activator in M1 and M2. Calcium hydroxide and sodium silicate were used as the alkali-activator in M3. The Blaine fineness of the GGBS used in this study was 4.204 cm^2/g and the maximum and average particle size of the GGBS was 76.3 μm and 8.5 μm, respectively. The specific gravity of GGBS was 2.93. Table 2 gives the chemical composition of GGBS measured from X-ray fluorescence (XRF) analysis; the molar ratio of the major elements in the source materials used was determined by energy-dispersive X-ray (EDX) analysis, with results listed in Table 3.

Several design principles gained from previous research on engineering strain-hardening cementitious composites [14–17] were adopted in ingredient selection in the present feasibility study of fiber reinforced alkali-activated mortar. Specifically, large aggregates, which lead to higher matrix toughness, are excluded from the mixture design. Following Li and coworkers [18,19], fine silica sand (100 μm average particle size) with a sand-to-binder (alkali-activated GGBS) ratio (S/B) of 0.4 by mass was used to maintain adequate composite stiffness and volume stability and to produce good workability. Using the approach suggested by Li [20], optimized amounts of the high-range water-reducing admixture (HRWRA) and the viscosity modifying admixture (VMA) were used to achieve the proper rheology to ensure uniform fiber dispersion. Antifoaming agent was included to minimize the amount of air bubbles. The specific amounts of these chemical admixtures for the three mixes M1–M3 are also given in Table 1. PVA fiber (2 vol.%) was used as reinforcement in all three mixes. The properties of the PVA fiber used in this study are listed in Table 4.

2.2. Mixing, casting, and curing of specimens

Each of the three compositions described above was mixed in a Hobart mixer. Solid ingredients, including binder and sand, were added to the mixer and mixed for approximately 3 min. Water was slowly added and the mixture was then mixed for another 3 min. Next, HRWRA, the antifoaming agent and VMA were added into the mixer for the achievement of proper viscosity of the matrix. Once a consistent mixture was reached, the fiber was gradually added, taking care to ensure uniform fiber dispersion. The whole mixing procedure for each batch generally took 10–15 min. Afterwards the mixture was cast into molds (six specimens for uniaxial tension test, two specimens for panel bending test, and three 50 mm cubes for cube compression test) while a moderate vibration was applied. The molds were covered with plastic sheets and cured in air at room temperature (23 °C ± 3 °C) for 1 day. The hardened specimens were then removed from the molds and cured in water until 28 days in a laboratory room at a temperature of 23 °C ± 3 °C.

Table 2
Chemical composition of the GGBS.

Material	SiO_2	Al_2O_3	Fe_2O_3	CaO	MgO	K_2O	TiO_2	SO_3	LOI[a]
GGBS	34.7	13.8	0.11	44.6	4.38	0.48	0.74	0.95	0.24

[a] Loss on ignition.

Table 3
Molar ratio of the major elements of the GGBS.

Material	Si/Al	Ca/Al	Si/Ca	Mg/Al	Mg/Ca	Mg/Si
GGBS	2.3	4.52	0.51	0.25	0.05	0.11

2.3. Density test

The hardened densities, ρ, were calculated by measuring their weight in air, W_{AIR}, and in water, W_{WATER}. The cubes were tested at 28 days in a water-saturated state with the excess water wiped from the surfaces:

$$\rho = \frac{W_{AIR}}{W_{AIR} - W_{WATER}} \times \rho_W \quad (1)$$

where ρ_W is the density of water assumed to be 1 g/cm^3.

2.4. Mechanical tests

Compressive strength was measured using 50 mm cube specimens according to ASTM C109-07 [22]. To investigate the behavior of the composites under tension, a series of uniaxial tension tests were performed by using an electronic universal testing machine. The tests were performed under displacement control with a loading speed of 0.1 mm/min, and the loading force and elongation were measured. Two linear variable differential transducers (LVDTs) were attached to both sides of the center of the tensile specimen with a gage length of 150 mm in order to monitor the elongation. The gage length refers to the distance between points A and B, as shown in Fig. 1b. The dimension of cross section within the gage length was 36 × 20 mm. To avoid fractures outside the gage length, both ends of the specimens were made with the dog-bone shape suggested by Kim et al. [23]. In addition to the tensile stress–strain curves, the ultimate tensile strength was measured, as was the ultimate tensile strain. More than four specimens were tested in order to check the variability of performance under tension.

A four-point panel bending test was conducted on all panel specimens measuring 400 mm × 100 mm × 10 mm to examine the flexural performance of the composites. The tests were performed under displacement control using an electronic universal testing machine. Four-point loading was applied, with the mid-span measuring 100 mm. The deflection at the center of the flexural specimens was measured by means of an LVDT at the center of each specimen. The flexural stress was calculated as

$$f_b = \frac{3P \times l}{b \times h^2} \quad (2)$$

where f_b is the flexural stress, P is the load, l is the distance between the supports and loading points, and b and h are the width and height of the specimen, respectively.

Table 1
Mix proportions.

Mixture ID	Binder		Sand	Water	HRWRA	VMA	Antifoamer	Fiber
	GGBS	Activator						
M1	0.895	0.105[a]	0.4	0.340	0.02	–	0.0002	0.02
M2	0.895	0.105[a]	0.4	0.438	–	0.0016	0.0002	0.02
M3	0.915	0.085[b]	0.4	0.382	0.03	–	0.0002	0.02

Note: All numbers are mass ratios of binder weight except fiber contents (volume fraction).
[a] Composition of 7.5% $Ca(OH)_2$ and 1% Na_2SO_4 relative to total binder by weight.
[b] Composition of 7.5% $Ca(OH)_2$ and 1% Na_2SiO_3 relative to total binder by weight.

Table 4
Properties of PVA fiber.

Fiber	Nominal strength[a] (MPa)	Fiber diameter (μm)	Fiber length (mm)	Young's modulus (GPa)	Elongation (%)	Oil coating (%)
REC15 PVA	1620	39	12	42.8	6.0	0.8

[a] Apparent fiber strength is 1092 MPa [21].

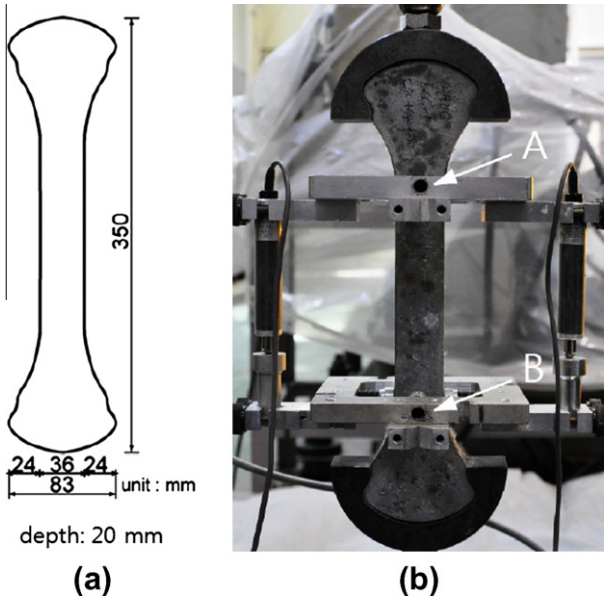

Fig. 1. Uniaxial tension test for: (a) the specimen geometry and (b) the uniaxial tension test setup.

3. Results and discussion

3.1. Density

Table 5 presents the hardened densities of each composite calculated by measuring the weight of three cubes in the water-saturated state. The theoretical densities calculated using the density of each composition and its proportion are 2.04 g/cm^3, 1.94 g/cm^3 and 1.98 g/cm^3 for M1, M2 and M3, respectively. Compared with the averaged measured values, the error rates are below 3%. These test results show that the new fiber reinforced cementless composite was successfully processed by the mixing procedure described in Section 2.2.

3.2. Compressive strength

Table 6 presents the 28 days compressive strength of each composite mix. As expected from the water to binder ratio, mixture M1 showed the highest compressive strength. All specimens showed different fracture behaviors compared with that of typical concrete. It is observed from Fig. 2 that propagation of cracks was restrained due to fiber-bridging resulting in a ductile mode of failure. In addition, the original shape of specimens remained after peak loading.

Table 5
Density at 28 days.

Mixture ID	Density (g/cm^3)
M1	2.01 ± 0.0227
M2	1.97 ± 0.142
M3	2.02 ± 0.157

Table 6
Compressive strength.

Mixture ID	Compressive strength (MPa)
M1	30.6 ± 4.42
M2	19.4 ± 3.16
M3	25.7 ± 3.22

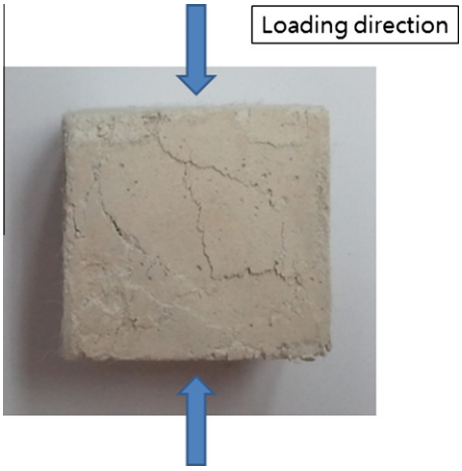

Fig. 2. Failure of compressive specimen.

3.3. Uniaxial tensile performance

The 28 days tensile stress–strain curves of the three composite mixes are shown in Fig. 3. All mixtures showed strain hardening behavior and clear ductility with multiple cracking. The values of the first cracking strength, tensile strength and tensile strain capacity of the three mixes are listed in Table 7. Mixture M1 showed the highest first cracking strength and tensile strength, with values 51.8% and 66.1%, respectively, higher than those of M2. These increases can be attributed to the low water to binder ratio for M1. The reason for the increase of tensile strength, which was higher than the first cracking strength, may be attributed to the interfacial properties, i.e. the chemical bonding energy and the frictional bond strength of M1 increased more than the cracking strength compared with M2, leading to higher fiber bridging strength. This can be verified with the fracture toughness test, single fiber pullout test [24] and micromechanical fiber bridging analysis [25,26]. The micromechanical investigation of the mortar and the interfacial properties of the fiber, reinforced cementless composite, will be studied in a follow-up investigation. The same phenomenon was observed in the comparison of M1 and M3. Mixture M1 showed the higher first cracking strength and tensile strength, which had values that were 5.93% and 12.2% higher than those for M3.

The average tensile strain capacity of mixture M1 was 4.48%, which value is similar to that of regular PVA-ECC [27], 224 times that of the same mortar (M1 without fiber with tensile strain capacity of 0.020%), 2.9 times that of M2, and 1.6 times that of M3.

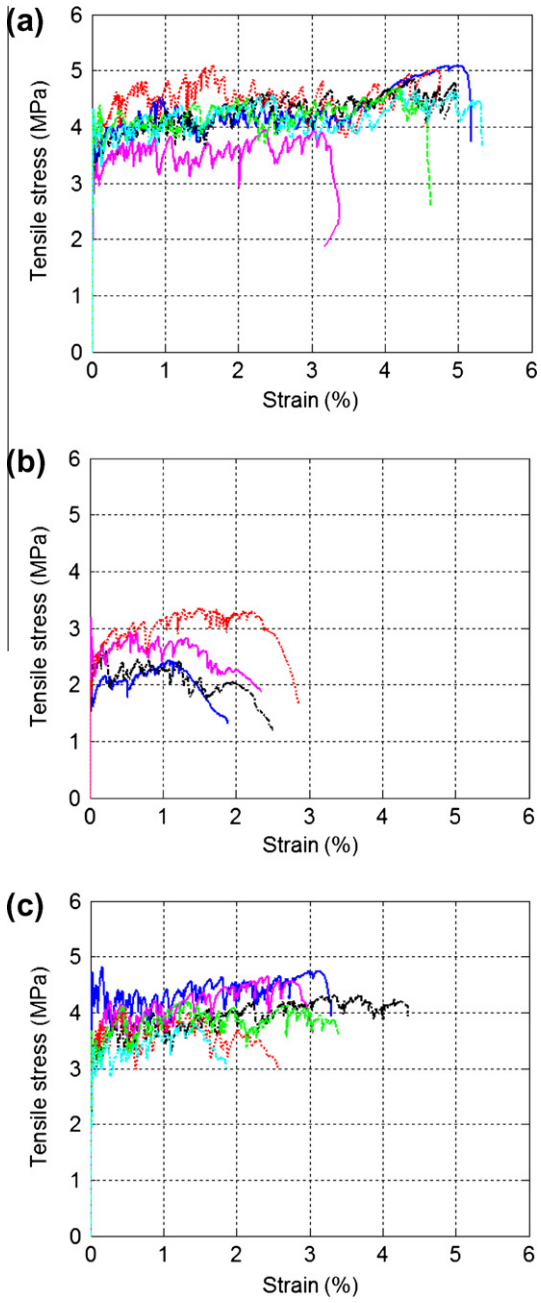

Fig. 3. Tensile stress vs. strain curve of: (a) M1, (b) M2, and (c) M3.

Table 7
Uniaxial tension test results.

Mixture ID	First cracking strength (MPa)	Tensile strength (MPa)	Tensile strain capacity (%)
M1	3.87 ± 0.464	4.69 ± 0.417	4.48 ± 0.767
M2	2.55 ± 0.541	2.83 ± 0.366	1.53 ± 0.486
M3	3.65 ± 0.546	4.18 ± 0.424	2.75 ± 0.939

According to previous works on ECC micromechanics [28–31], two criteria should be satisfied in order to achieve pseudo strain-hardening behavior based on multiple cracking. The matrix tensile cracking strength σ_c must not exceed the maximum fiber bridging strength σ_0. The strength-based criterion must control the initiation of crack propagation from the material defect sites. If this condition is satisfied, an immediate stress drop after initial cracking with bridging fibers being pulled out or ruptured is prevented. Instead, multiple cracking with increasing load occurs. Apart from the strength criterion, another condition for pseudo strain-hardening is that the crack tip toughness J_{tip} must be less than the complementary energy J_b', calculated from the fiber bridging stress σ vs. crack opening δ curve. Satisfaction of the energy-based criterion is necessary to assure the steady-state flat crack propagation mode and the multiple cracking phenomenon. Kanda and Li [32] proposed performance indices σ_0/σ_{fc} (stress performance index) and J_b'/J_{tip} (energy performance index) for the condition of saturated pseudo strain-hardening (PSH) behavior. If both these performance indices exceed unity, the PSH behavior can theoretically be achieved. However, the potential of higher tensile strain capacity increases with higher performance indices. With respect to the stress performance index, the mixture M1 showed a stress performance index of 1.21. The mixtures M2 and M3 showed values of 1.11 and 1.15, respectively. This is the reason for the higher tensile strain capacity of M1 compared with that of M2 or M3. For a detailed analysis of the satisfaction of the strength and energy criteria for these composites, it will be necessary to perform fracture toughness test, single fiber pullout test and micromechanical fiber bridging analysis, which is outside the scope of this feasibility study.

Fig. 4 shows the crack patterns of M1. Multiple micro-cracks with a crack spacing of 2–3 mm were observed. Crack widths were measured using a microscope. The cracks of M1 had an averaged residual width of 20.2 μm, measured from the unloaded specimen after uniaxial tension testing. The loaded crack width of 100 μm was calculated from the number of cracks, the crack spacing and the tensile strain capacity of M1. The averaged loaded and residual crack widths for M2 were 45.9 μm and 25.3 μm, respectively. Although showing a small crack width in M2, the crack distribution was not uniform and unsaturated cracking behavior is observed. The averaged loaded and residual crack widths for M3 are 68.8 μm and 28.7 μm, respectively.

When compared across the three mixtures, the residual crack widths are much remarkably similar, while the loaded crack widths are quite different. The loaded crack width is the crack opening corresponding to maximum bridging stress in the fiber bridging curve. From these observations the crack opening corresponding to maximum bridging stress of M1 is largest among all mixtures. In addition, comparison of the tensile strength reached in the composites (Fig. 3) suggests that the peak bridging stress for M1 is highest among all mixtures. The high bridging stress and crack opening in M1 suggest that the complementary energy

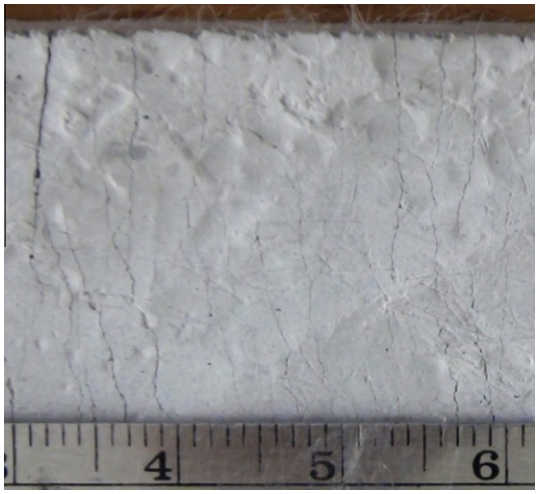

Fig. 4. Multiple micro-cracks of M1 (unit: mm).

of M1 is the largest among the three mixtures. Assuming a similar value for J_{tip} for all mixtures, this translates into a higher energy performance index for M1 compared to the other mixtures. Thus, with the highest stress performance and energy performance indices, it is not surprising that M1 develops the highest tensile ductility, as expected theoretically.

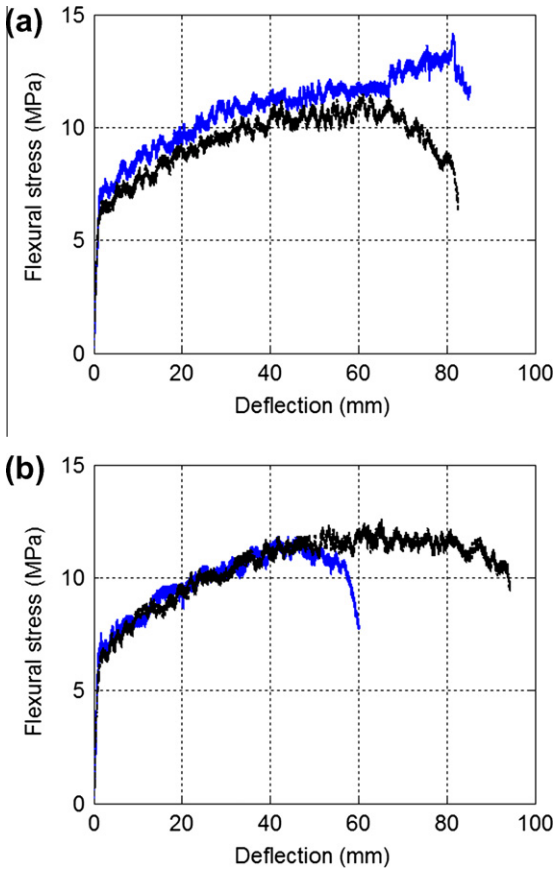

Fig. 5. Flexural stress vs. deflection curve of: (a) M1 and (b) M3.

Table 8
Panel bending test results.

Mixture ID	Flexural strength (MPa)	Deflection (mm)
M1	12.7 ± 1.93	74.3 ± 10.3
M2	–	–
M3	11.9 ± 0.806	58.6 ± 9.55

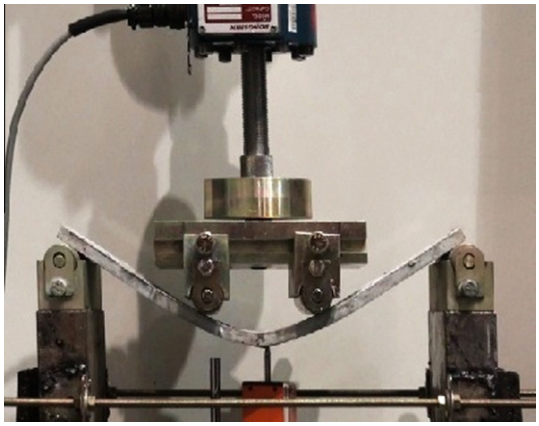

Fig. 6. High-ductile behavior of M1 specimen in bending.

3.4. Flexural performance

Fig. 5 shows the 28 days flexural stress–deflection curves of mixtures M1 and M3. (M2 was not tested in bending given the relatively low tensile ductility.) All specimens showed deflection hardening behavior with multiple cracking. The flexural strength and corresponding deflection are listed in Table 8. The mixture M1 exhibited higher flexural strength and deflection than M3, reflecting the higher tensile strength and strain capacity of M1 in the uniaxial tension tests. Fig. 6 presents the typical behavior of M1 in bending, showing extremely high ductility.

4. Conclusions

This paper presents a feasibility study of strain-hardening fiber reinforced cementless composite using alkali-activated ground blast furnace slag based mortar and PVA fibers. A series of experimental tests was carried out to investigate the mechanical properties and density. From the test results, it was demonstrated that tensile strain hardening behavior and ductility as high as 4.7% can be attained. Specifically, for the three mixtures with different alkali-activators and water to binder ratios, the tensile strain capacity ranged from 1.53% to 4.48%, the first cracking strength ranged from 2.55 MPa to 3.87 MPa, and the tensile strength ranged from 2.83 MPa to 4.69 MPa at 28 days. The hardened density ranged from 1.97 g/cm^3 to 2.02 g/cm^3. It was found that the tensile strain capacity increases with an increase of the stress performance index (the ratio of peak bridging stress to first cracking strength) and energy performance index (the ratio of complementary energy to matrix fracture toughness). The mixture M1, with an alkali-activator of $Ca(OH)_2$ and Na_2SO_4, and a water to binder ratio of 0.34, exhibited excellent mechanical performance compared with that of mixture M2 and mixture M3 in terms of compressive strength, tensile strength, and tensile ductility. M1 exhibited a compressive strength of 30.6 MPa, a tensile strength of 4.69 MPa, a tensile strain capacity of 4.48%, a flexural strength of 12.7 MPa, and a corresponding flexural deflection of 74.3 mm, with specimen dimensions of 400 mm × 100 mm × 10 mm. These experimental data verify that strain-hardening and high tensile ductility in fiber reinforced alkali-activated slag mortar can be achieved without a doubt, despite the high brittleness of the slag mortar itself.

While the data presented in this article are encouraging, a more systematic study of the micromechanical parameters including matrix toughness and fiber/matrix interfacial properties should be carried out to fully understand the fundamental mechanisms supporting strain-hardening in these composites, and the underlying reasons for the differences in mechanical properties observed in these three mixes. The strain-hardening feasibility established in the present study warrants more detailed investigations into optimized composite design and durability characteristics of this new class of cementless composites for potential applications in future eco-friendly civil infrastructure.

Acknowledgements

This work was supported by Basic Science Research Program through the National Research Foundation of Korea (NRF) funded by the Ministry of Education, Science and Technology (No. 2011-0020027). V.C. Li acknowledges support from the US National Science Foundation (Grant CMMI 1068005 to the University of Michigan).

References

[1] Damtoft JS, Lukasik J, Herfort D, Sorrentino D, Gartner EM. Sustainable development and climate change initiatives. Cem Concr Res 2008;38:115–27.
[2] Malhotra VM. Introduction: sustainable development and concrete technology. Concr Int 2001;24(7):22.
[3] Pacheco-Torgal F, Castro-Gomes J, Jalali S. Alkali activated binders: a review. Part 2—About materials and binder manufacture. Constr Build Mater 2007;22(7):1305–14.
[4] Palomo A, Grutzeck MW, Blanco MT. Alkali-activated fly ashes: a cement for the future. Cem Concr Res 1999;29(8):1323–9.
[5] Wang S, Pu SC, Scrivener KL, Ptatt PL. Alkali activated slag cement and concrete: a review of properties and problems. Adv Cem Res 1995;27:93–102.
[6] Collins FG, Sanjayan JG. Workability and mechanical properties of alkali activated slag concrete. Cem Concr Res 1999;29(3):455–8.
[7] Yang KH, Song JK, Ashour AF, Lee ET. Properties of cementless mortar activated by sodium silicate. Constr Build Mater 2008;22(8):1981–9.
[8] Oh JE, Monteiro PJM, Jun SS, Choi S, Clark SM. The evolution of strength and crystalline phases for alkali-activated ground blast furnace slag and fly ash-based geopolymers. Cem Concr Res 2010;40(2):189–96.
[9] Ji YJ. The fracture properties of alkali-slag concrete. In: International symposium on concrete engineering, Nanjing, PR China, 1991. p. 459–64.
[10] Kim JK, Lee Y, Yi ST. Fracture characteristics of concrete at early ages. Cem Concr Res 2004;34(3):507–19.
[11] Savastano Jr H, Warden PG, Coutts RSP. Potential of alternative fibre cements as building materials for developing areas. Cem Concr Res 2003;25(6):585–92.
[12] Silva FJ, Thaumaturgo C. Fibre reinforcement and fracture response in geopolymeric mortars. Fatigue Fract Eng Mater Struct 2003;26:167–72.
[13] Dias DP, Thaumaturgo C. Fracture toughness of geopolymeric concretes reinforced with basalt fibers. Cem Concr Compos 2003;27:49–54.
[14] Marshall DB, Cox BN. A J-integral method for calculating steadystate matrix cracking stressed in composites. Mech Mater 1988;7(2):127–33.
[15] Leung CKY. Design criteria for pseudoductile fiber-reinforced composites. ASCE J Eng Mech 1996;122(1):10–4.
[16] Li VC, Leung CKY. Steady-state and multiple cracking of short random fiber composites. ASCE J Eng Mech 1992;118(11):2246–64.
[17] Yang EH, Li VC. Strain-hardening fiber cement optimization and component tailoring by means of a micromechanical model. Constr Build Mater 2010;24:130–9.
[18] Li VC, Mishra DK, Wu C. Matrix design for pseudo strain-hardening fiber reinforced cementitious composites. Mater Struct 1995;28(183):586–95.
[19] Fischer G, Li VC. Design of engineered cementitious composites (ECCs) for processing and workability requirement. Poland: Proc BMC 2003;7:29–36.
[20] Li M. Multi-scale design for durable repair of concrete structures. PhD thesis: The University of Michigan; 2009.
[21] Li VC, Wu C, Wang S, Ogawa A, Saito T. Interface tailoring for strain-hardening polyvinyl alcohol-engineered cementitious composites (PVA-ECCs). ACI Mater J 2002;99(5):463–72.
[22] ASTM. Standard test method for compressive strength of hydraulic cement mortars (using 50 mm [2 in.] cube specimens). ASTM C109/C109M-07; 2007.
[23] Kim JK, Kim JS, Ha GJ, Kim YY. Tensile and fiber dispersion performance of ECC (Engineered Cementitious Composites) produced with ground granulated blast furnace slag. Cem Concr Res 2007;37(7):1096–105.
[24] Redon C, Li VC, Wu C, Hoshiro H, Saito T, Ogawa A. Measuring and modifying interface properties of PVA fibers in ECC Matrix. ASCE J Mater Civil Eng 2001;13(6):399–406.
[25] Lin Z, Li VC. Crack bridging in fiber reinforced cementitious composites with Slip-hardening Interfaces. J Mech Phys Solids 1997;45(5):763–87.
[26] Yang EH, Wang S, Yang Y, Li VC. Fiber-bridging constitutive law of engineered cementitious composites. J Adv Concr Technol 2008;6(1):181–93.
[27] Li VC, Wang S, Wu C. Tensile strain-hardening behavior of polyvinyl alcohol-engineered cementitious composite (PVA-ECC). ACI Mater J 2001;98(6):483–92.
[28] Li VC, Wu C. Conditions for pseudo strain hardening in fiber reinforced brittle matrix composites. J Appl Mech Rev. 1992;45(8):390–8.
[29] Li VC, Leung CKY. Theory of steady state and multiple cracking of random discontinuous fiber reinforced brittle matrix composites. J Eng Mech-ASCE 1992;118(11):2246–64.
[30] Leung CKY. Design criteria for pseudoductile fiber-reinforced composites. J Eng Mech-ASCE 1996;122(1):10–4.
[31] Li VC, Wang S. Microstructure variability and macroscopic composite properties of high performance fiber reinforced cementitious composites. Probab Eng Mech 2006;21(3):201–6.
[32] Kanda T, Li VC. Practical design criteria for saturated pseudo strain hardening behavior in ECC. J Adv Concr Technol 2006;4(1):59–72.